Atmos. Chem. Phys. Discuss., 11, 21631–21654, 2011
www.atmos-chem-phys-discuss.net/11/21631/2011/
doi:10.5194/acpd-11-21631-2011

Atmospheric Chemistry and Physics Discussions

A hybrid bin scheme to solve the condensation/evaporation equation using a cubic distribution function

T. Dinh and D. R. Durran

Department of Atmospheric Sciences, University of Washington, Seattle, WA 98195, USA

Received: 20 July 2011 – Accepted: 22 July 2011 – Published: 1 August 2011

Correspondence to: T. Dinh (tradinh@uw.edu)

Published by Copernicus Publications on behalf of the European Geosciences Union.

Abstract

A computationally efficient method is proposed to replace the piecewise linear number distribution in a hybrid bin scheme with a piecewise cubic polynomial. When the linear distribution is replaced by a cubic, the errors generated in solutions to the condensation/evaporation equation are reduced by a factor of two to three. Alternatively, using the cubic distribution function allows reducing the number of bins by 20 ± 5 % when solving the condensation/evaporation problem without sacrificing accuracy.

1 Introduction

In the microphysics context, a hybrid bin scheme is a two-moment explicit scheme designed to solve for the evolution of the size spectrum of cloud droplets and ice crystals. The particular hybrid bin scheme that is the focus of this paper is the scheme developed by Chen and Lamb (1994); hereafter referred to as the CL scheme.

The CL scheme has been implemented in meso- and synoptic-scale cloud resolving models, including the Nonhydrostatic Modeling System of the University of Wisconsin (Hashino and Tripoli, 2007) and the Goddard Cumulus Ensemble model (Przyborski, 2006). It has also been used in case studies of warm clouds (Kuba and Fujiyoshi, 2006; Kuba and Murakami, 2010), orographic clouds (Chen and Lamb, 1999), synoptically forced cirrostratus (Lin et al., 2005) and thin cirrus in the tropical tropopause layer (Dinh et al., 2010).

The CL scheme produces less numerical diffusion than one-moment bin schemes and so is more accurate. Yet, because of its computational cost, it has not been implemented in 3-D or large-scale models. In the CL scheme, the evolution of two moments (mass and number of particles) in each bin has to be evaluated, which can impose both computational and storage burdens in dynamically-coupled multidimensional cloud models.

ACPD
11, 21631–21654, 2011

The CL scheme is based on a linear fit to the number distribution of microphysical particles in each bin. In this paper, we show that replacing the linear distribution function by a cubic polynomial significantly reduces the error of the scheme in solving the condensation/evaporation equation. This new scheme can be used to increase accuracy, or can alternatively allow computations with fewer bins to obtain the same accuracy. Such an increase in efficiency may be useful for modelers using hybrid bin schemes in cloud resolving models.

2 The hybrid bin scheme

2.1 Evolution of the number density

The evolution of the number density $n = n(\boldsymbol{x}, m, t)$ of microphysical particles (droplets or crystals) is described by

$$\frac{\partial n}{\partial t} = -\nabla \cdot (\boldsymbol{u} n) + \frac{\partial}{\partial z}(V_t n) - \frac{\partial}{\partial m}(cn) + G \tag{1}$$

where $\boldsymbol{x} = (x, y, z)$ is the vector location in space, m is the particle mass and t is time. The first term in Eq. (1) is advection in space by the velocity vector $\boldsymbol{u}$. The second term is sedimentation of particles at the terminal fall speed V_t. The third term is growth at rate c by water vapor condensation onto droplets or deposition onto crystals. The last term G represents the aggregation process.

In a cloud resolving model, the changes in n due to the individual terms in Eq. (1) are computed separately and then summed together to give n at the next time step. Here we will concentrate on the condensation/deposition term only.

ACPD
11, 21631–21654, 2011

2.2 Subgrid linear distribution

In the original CL scheme, the number density n as a function of the mass of particles m in each bin is assumed linear and represented by

$$n(m) = n_0 + k(m - m_0), \tag{2}$$

and the total number and mass of particles in the bin are given as

$$\mathcal{N} = \int_{m_1}^{m_2} n(m)\mathrm{d}m, \quad \mathcal{M} = \int_{m_1}^{m_2} mn(m)\mathrm{d}m, \tag{3}$$

where m_1 and m_2 are the masses that define the bin boundaries. Equations (2) and (3) are consistent when

$$n_0 = \frac{\mathcal{N}}{\Delta m}, \quad k = \frac{12\mathcal{N}(\overline{m} - m_0)}{(\Delta m)^3}, \tag{4}$$

where $m_0 = (m_1 + m_2)/2$, $\Delta m = m_2 - m_1$ and $\overline{m} = \mathcal{M}/\mathcal{N}$ is the mean mass of the bin.

The distribution function given by Eqs. (2) and (3) may be negative in part of the bin. If that happens Chen and Lamb (1994) ensured positiveness by modifying the distribution so that it occupies only part of the bin. If $n_0 + k(m_1 - m_0) < 0$, they set

$$n(m) = \begin{cases} k_*(m - m_*) & \text{if} \quad m_* \le m \le m_2, \\ 0 & \text{otherwise}, \end{cases} \tag{5}$$

where[1]

$$m_* = 3\overline{m} - 2m_2, \quad k_* = \frac{2\mathcal{N}}{(m_2 - m_*)^2}.$$

[1]There is an error in the formula for k_* in Chen and Lamb (1994). The correct formula for k_* is given here.

ACPD
11, 21631–21654, 2011

Alternatively, if $n_0 + k(m_2 - m_0) < 0$,

$$n(m) = \begin{cases} k_*(m - m_*) & \text{if} \quad m_1 \le m \le m_*, \\ 0 & \text{otherwise}, \end{cases} \tag{6}$$

where

$$m_* = 3\overline{m} - 2m_1, \quad k_* = -\frac{2\mathcal{N}}{(m_1 - m_*)^2}.$$

2.3 Bin shift

Let N be the number of bins and $\mu_1, \mu_2, \ldots, \mu_{N+1}$ denote the grid divisions along the mass axis. In both the original CL algorithm and our new method, the procedure to step $\mathcal{N}_j$ and $\mathcal{M}_j$ forward in time for each bin j involves growing the particles in the bin, shifting the bin along the mass axis and finally mapping the shifted bin onto the mass axis. The algorithm may be described by the following four steps:

1. The number and mass after one step of condensational/depositional growth in bin j are calculated as

$$\tilde{\mathcal{N}}_j = \mathcal{N}_j,$$
$$\tilde{\mathcal{M}}_j = \mathcal{M}_j + \mathcal{N}_j c(\overline{m}_j)\Delta t,$$

where $c(\overline{m}_j)$ is the growth rate at the mean mass $\overline{m}_j = \mathcal{M}_j / \mathcal{N}_j$. For efficiency, all particles in the bin are assumed to grow at the rate of the mean mass of the bin.

2. The left and right boundaries of the shifted bin ($m_{1,j}$ and $m_{2,j}$) are calculated as:

$$m_{1,j} = \mu_j + c(\mu_j)\Delta t, \quad m_{2,j} = \mu_{j+1} + c(\mu_{j+1})\Delta t,$$

where $c(\mu_j)$ and $c(\mu_{j+1})$ are the growth rate at the mass values μ_j and μ_{j+1}.

ACPD
11, 21631–21654, 2011

3. In the original CL scheme, the linear number distribution within each shifted bin is computed from $\tilde{\mathcal{N}}_j$, $\tilde{\mathcal{M}}_j$, $m_{1,j}$ and $m_{2,j}$ using Eqs. (2), (4), (5) and (6). The new procedure using the cubic distribution is discussed in the next section.

4. Find the location of the shifted bin with respect to the grid by comparing $m_{1,j}$ and $m_{2,j}$ with the grid points $\mu_1, \mu_2, \ldots, \mu_{N+1}$. For each grid bin overlapped by the shifted bin, integrate the distribution function of the shifted bin to find the number and mass of particles that will be accumulated in the grid bin. See Chen and Lamb (1994) for illustrations.

2.4 Subgrid cubic distribution

The slope of the linear distribution function in each bin does not depend on the distribution in adjacent bins. As in higher-order finite volume methods, the distribution within in each bin can be more accurately estimated using information from adjacent bins. A cubic polynomial representing the number distribution in each bin can be evaluated using information from the bins immediately to the right and left (in addition to the total number and mass of the centered bin).

Chen and Lamb (1994) mentioned the possibility of using higher-order polynomial distributions that were continuous across bin boundaries. However, continuity at the bin boundary is not the optimal approach because, compared with other points along the mass axis within the bin, the boundaries of the bin are subject to the largest error. Indeed, the assumption that the growth rate of particles in the bin is equal to the growth rate of the mean mass is least accurate at the bin boundaries. The *growth-of-the-mean* assumption, though essential to the efficiency of the CL scheme, introduces large errors at the boundaries and occasionally causes the distribution to become negative there.

Hence, to derive the cubic form of the distribution for each bin, it is best to avoid using the additional data at the bin boundaries. Instead, we use of the values of the number distribution at the mean masses in the two adjacent bins. The value of the

ACPD
11, 21631–21654, 2011

distribution at the mean mass, denoted here by $\overline{n}$, can be approximated by the linear form of the distribution, i.e. by evaluating Eqs. (2), (5) or (6) at the mean mass value.

Suppose that we represent the number distribution in each bin as the cubic

$$n(m) = a_0 + a_1 m + a_2 m^2 + a_3 m^3. \tag{7}$$

The coefficients $a_0, \ldots, a_3$ are to be determined by the conservation of number and mass (Eq. 3) in the centered bin, and by requiring that $(\overline{m}_L, \overline{n}_L)$ and $(\overline{m}_R, \overline{n}_R)$ from the left and right bins satisfy Eq. (7). Here, we need to solve a system of linear equations for four coefficients $a_0, \ldots, a_3$ for each bin.

An economical solution procedure can be obtained by rewriting the number distribution as a weighted sum of the four lowest order Legendre polynomials, which are

$$P_0(\chi) = 1, \tag{8}$$

$$P_1(\chi) = \chi, \tag{9}$$

$$P_2(\chi) = \frac{1}{2}(3\chi^2 - 1), \tag{10}$$

$$P_3(\chi) = \frac{1}{2}(5\chi^3 - \chi), \tag{11}$$

where χ is an independent variable defined between -1 and 1. A key property of the Legendre polynomials is the orthogonality condition,

$$\int_{-1}^{1} P_j P_k \, \mathrm{d}\chi = \frac{2}{2j+1}\delta_{jk}, \tag{12}$$

where δ_{jk} denote the Kronecker delta. If we define χ as

$$\chi = \frac{2(m - m_0)}{m_2 - m_1}, \tag{13}$$

ACPD
11, 21631–21654, 2011

then as m varies between m_1 and m_2, χ varies between -1 and 1. Now the distribution function can be written as a function of χ:

$$n(\chi) = b_0 P_0(\chi) + b_1 P_1(\chi) + b_2 P_2(\chi) + b_3 P_3(\chi). \tag{14}$$

Based on the orthogonality property (Eq. 12), the conservation of number and mass (Eq. 3) simplifies to

$$\begin{aligned}
\mathcal{N} &= \frac{\Delta m}{2}\int_{-1}^{1}(b_0P_0 + b_1P_1 + b_2P_2 + b_3P_3)P_0\,\mathrm{d}\chi \\
&= b_0\Delta m, \\
\mathcal{M} &= \frac{\Delta m}{2}\int_{-1}^{1}(b_0P_0 + b_1P_1 + b_2P_2 + b_3P_3)\left(m_0P_0 + \frac{\Delta m}{2}P_1\right)\mathrm{d}\chi \\
&= \frac{\Delta m}{2}\left(2m_0b_0 + \frac{\Delta m}{3}b_1\right),
\end{aligned}$$

from which

$$b_0 = \frac{\mathcal{N}}{\Delta m}, \tag{15}$$

$$b_1 = \frac{6(\mathcal{M} - m_0\mathcal{N})}{(\Delta m)^2}. \tag{16}$$

Note that when $b_2 = 0$ and $b_3 = 0$, these values of b_0 and b_1 are consistent with the linear distribution function given by Eqs. (2) and (4).

Next b_2 and b_3 are determined by requiring that $(\chi(\overline{m}_\mathrm{L}), \overline{n}_\mathrm{L})$ and $(\chi(\overline{m}_\mathrm{R}), \overline{n}_\mathrm{R})$ from the left and right bins satisfy Eq. (14). $\chi(\overline{m}_\mathrm{L})$ and $\chi(\overline{m}_\mathrm{R})$ are Eq. (13) evaluated at the mean masses of the left and right bins. This means

ACPD
11, 21631–21654, 2011

$$b_0 + b_1\overline{\chi}_L + b_2\frac{3\overline{\chi}_L^2 - 1}{2} + b_3\frac{5\overline{\chi}_L^3 - 3\overline{\chi}_L}{2} = \overline{n}_L, \quad (17)$$

$$b_0 + b_1\overline{\chi}_R + b_2\frac{3\overline{\chi}_R^2 - 1}{2} + b_3\frac{5\overline{\chi}_R^3 - 3\overline{\chi}_R}{2} = \overline{n}_R, \quad (18)$$

where

$$\overline{\chi}_L = \chi(\overline{m}_L) = \frac{2(\overline{m}_L - m_0)}{m_2 - m_1}, \quad \overline{\chi}_R = \chi(\overline{m}_R) = \frac{2(\overline{m}_R - m_0)}{m_2 - m_1}.$$

Equations (17) and (18) are two linear equations of two unknowns (b_2 and b_3), which can be solved easily to obtain b_2 and b_3.

Finally, the coefficients for the cubic distribution function in standard form are obtained by substituting Eqs. (8)–(11) and (13) into Eq. (14) and comparing with Eq. (7):

$$a_0 = b_0 - 2qb_1 + \left(6q^2 - \frac{1}{2}\right)b_2 - \left(20q^3 - 3q\right)b_3, \quad (19)$$

$$a_1 = \frac{2b_1 - 12qb_2 + \left(60q^2 - 3\right)b_3}{\Delta m}, \quad (20)$$

$$a_2 = \frac{6b_2 - 60qb_3}{(\Delta m)^2}, \quad (21)$$

$$a_3 = \frac{20b_3}{(\Delta m)^3}, \quad (22)$$

where $q = \frac{m_0}{\Delta m}$.

The cubic distribution function may be negative in part of the bin, in which case it should be rejected and the linear form (Eqs. 2, 5 or 6) should be used. This is the case if either of the followings occurs:

ACPD
11, 21631–21654, 2011

– The cubic distribution function obtains a negative minimum inside the bin, i.e., if

$$\Delta = a_2^2 - 3a_1a_3 \geq 0$$

and for $m_e = \frac{-a_2+\sqrt{\Delta}}{3a_3}$, we have $m_1 \leq m_e \leq m_2$ and

$$n(m_e) = a_0 + a_1 m_e + a_2 m_e^2 + a_3 m_e^3 < 0.$$

– The cubic distribution function is negative at the left and/or the right bin boundaries, which is the case if

$$n(m_1) = a_0 + a_1 m_1 + a_2 m_1^2 + a_3 m_1^3 < 0,$$

or

$$n(m_2) = a_0 + a_1 m_2 + a_2 m_2^2 + a_3 m_2^3 < 0.$$

The only modification to the bin-shift procedure outlined in Sect. 2.3 is in Step 3, which is replaced by

3. Compute the cubic distribution function using Eqs. (15)–(22), and use this distribution if it is nonnegative. Otherwise use the linear distribution. The linear distribution function should also be used for the leftmost and rightmost bins.

3 Numerical tests

3.1 Evaporation of cloud drops

The extra work required to determine the coefficients for the cubic number distribution is very modest owing to the orthogonality of the Legendre polynomials. In this section we examine the increases in accuracy provided by the new piecewise cubic scheme.

ACPD
11, 21631–21654, 2011

3.1.1 Initial conditions

For dilute and relatively large spherical drops, the condensational growth rate can be approximated by

$$c = \frac{\mathrm{d}m}{\mathrm{d}t} = BSm^{1/3}, \tag{23}$$

where S is the supersaturation ratio and $B = 4.7 \times 10^{-8}\,\mathrm{kg}^{2/3}\,\mathrm{s}^{-1}$ under standard temperature and pressure.

The initial drop spectrum is assumed to be

$$f(m) = \frac{N_0 m}{m_c^2} \exp\left(-\frac{m}{m_c}\right), \tag{24}$$

where $N_0 = 2.0 \times 10^8\,\mathrm{m}^{-3}$ and m_c is the mode of the distribution (where $f(m)$ is maximum). We set $m_c = 3.5 \times 10^{-8}\,\mathrm{kg}$, which is the mass of a drop whose radius is 200 µm.

The analytical solution to the evolution of the drop spectrum when the growth rate is given by Eq. (23) was derived by Tzivion et al. (1989). It is

$$n(m,t) = m^{-1/3} X^{1/2} f\left(X^{3/2}\right), \tag{25}$$

where $X = m^{2/3} - \frac{2}{3}BSt$ and $f(X^{3/2})$ is the initial drop spectrum function evaluated at $X^{3/2}$.

Numerical solutions are computed for the case when drops evaporate at fixed $S = -0.20$.

ACPD
11, 21631–21654, 2011

3.1.2 Grid and time spacings

The grid points along the mass axis μ_j for $j = 1,2,\ldots,N+1$, where N is the number of bins, are defined by

$$\mu_j = \frac{4}{3}\rho\pi r_j^3,$$

$$r_j = r_{\min}\alpha^{j-1},$$

$$\alpha = \left(\frac{r_{\max}}{r_{\min}}\right)^{1/N},$$

where $r_{\min} = 1\,\mu\text{m}$ and $r_{\max} = 1000\,\mu\text{m}$. The grid thus spans between $r_{\min}$ and $r_{\max}$ and is more tightly spaced for small radii.

The time step is $\Delta t = 1\,\text{s}$.

3.1.3 Results

Solutions for the evaporation problem at 20-bin-resolution at 50 min are shown in Fig. 1a (number of drops per bin) and b (mass of drops per bin). The solution obtained by the cubic scheme is more accurate than that by the linear scheme. In particular, the linear scheme underestimates the number and mass of larger drops (with major errors in bin 17). At this resolution, the root-mean-square errors of the linear and cubic schemes are respectively $1.22 \times 10^6\,\text{m}^{-3}$ and $0.64 \times 10^6\,\text{m}^{-3}$ in cloud drop number and $6.34 \times 10^{-2}\,\text{kg}\,\text{m}^{-3}$ and $2.29 \times 10^{-2}\,\text{kg}\,\text{m}^{-3}$ in drop mass.

The errors of the solutions obtained by the linear and cubic schemes are given as a function of bin resolution in Table 1 and Fig. 2. At all but the coarsest resolution (10 bins) the errors produced by the cubic scheme are about half of those by the linear scheme.

ACPD
11, 21631–21654, 2011

3.2 Depositional growth of small ice crystals

3.2.1 Initial conditions

If ice crystals are assumed spherical, the depositional growth rate can be calculated as

$$c = \frac{\mathrm{d}m}{\mathrm{d}t} = \frac{4\pi r S_{\mathrm{ice}}}{\frac{R_{\mathrm{v}}T}{e_{\mathrm{sat,ice}}D'_{\mathrm{v}}} + \frac{L_{\mathrm{s}}}{k'_{\mathrm{a}}T}\left(\frac{L_{\mathrm{s}}}{R_{\mathrm{v}}T} - 1\right)} \tag{26}$$

(Pruppacher and Klett, 1978, p. 448), where m and r are respectively the mass and radius of ice crystals, R_{v} is the gas constant for water vapor, L_{s} is the latent heat of sublimation, k'_{a} is the modified thermal conductivity of air, D'_{v} is the modified diffusivity of water vapor in air, $e_{\mathrm{sat,ice}}$ is the saturation vapor pressure over plane ice surface, S_{ice} is the supersaturation ratio with respect to ice and T is temperature. Here we will consider the case of ice crystals in thin cirrus in the tropical tropopause layer, where typically $p = 100\,\mathrm{mb}$ and $T = 193\,\mathrm{K}$.

The supersaturation ratio is $S_{\mathrm{ice}} = 0.40$ initially. In supersaturated condition, S_{ice} will decrease with time as water vapor is deposited onto ice crystals.

There is no analytical solution for this case. To evaluate the performance of the linear and cubic schemes, numerical solutions obtained by these schemes at low resolution are compared with a numerical solution obtained by either of these schemes at high resolution. At high resolution both schemes converge to the same result, so either scheme can be used to obtain the high resolution solution.

The initial crystal spectrum is assumed to be Eq. (24), where $N_0 = 5.0 \times 10^5\,\mathrm{m}^{-3}$ and $m_c = 2.5 \times 10^{-13}\,\mathrm{kg}$. The latter is the mass of a crystal whose radius is 4 µm.

ACPD
11, 21631–21654, 2011

3.2.2 Grid and time spacings

The grid points along the mass axis μ_j for $j = 1, 2, \ldots, N+1$, where N is the number of bins, are defined by

$$\mu_j = \frac{4}{3}\rho\pi r_j^3,$$
$$r_j = r_{\min} + \alpha(j-1),$$
$$\alpha = \frac{r_{\max} - r_{\min}}{N},$$

where $r_{\min} = 0.3\,\mu m$ and $r_{\max} = 12\,\mu m$. $r_{\max} = 12\,\mu m$ is sufficiently large for this case because during the simulation there is no ice crystal that grows to a radius larger than 12 µm. The grid thus spans between $r_{\min}$ and $r_{\max}$ and is equally spaced in terms of radii of ice crystals. An equally spaced grid is possible in this case because the range of ice crystal sizes to be covered by the grid is narrow (between 0.3 µm and 12 µm).

The time step is $\Delta t = 1\,s$.

3.2.3 Results

The supersaturation ratio S_{ice} decreases from 0.40 at the initial time to 0.076 at 30 min.

Numerical solutions at 6-bin-resolution at 30 min are shown in Fig. 3a (number of crystals per bin) and b (mass of crystals per bin). The solution obtained by the cubic scheme is more accurate than that by the linear scheme. At this resolution, the root-mean-square errors of the linear and cubic schemes are respectively $9.57 \times 10^3\ m^{-3}$ and $2.87 \times 10^3\ m^{-3}$ in crystal number and $1.67 \times 10^{-8}\ kgm^{-3}$ and $0.50 \times 10^{-8}\ kgm^{-3}$ in crystal mass. Compared with the high resolution solution and the cubic scheme, the linear scheme overestimates the maximum mass in bin 4 and underestimates the masses in the bins adjacent to the maximum (bins 3 and 5).

ACPD
11, 21631–21654, 2011

The errors of the solutions obtained by the linear and cubic schemes are given as a function of bin resolution in Table 2 and Fig. 4. The errors of the cubic scheme are typically about a third of those of the linear scheme.

The error reduction due to the cubic scheme means that the number of bins can be reduced without sacrificing accuracy. For the same accuracy, the number of bins required for the cubic scheme is 20 ± 5 % less than that of the linear scheme. This is estimated as the difference in the intercepts of a horizontal line (whose value is the desired error) with the error curves of the cubic and linear schemes in Figs. 2 and 4.

4 Summary

We have presented a computationally efficient method to replace the piecewise linear number distribution in the hybrid bin scheme originally developed by Chen and Lamb (1994) with a piecewise cubic polynomial. For models in which the CL scheme has been implemented, migrating from the linear distribution function to the cubic distribution should be relatively simple.

When the original linear distribution is replaced by a cubic, the errors generated in solutions to the condensation/evaporation equation are reduced by a factor of two to three. Alternatively, using the cubic distribution function would allow reducing the number of bins by 20 ± 5 % when solving the condensation/evaporation problem without sacrificing accuracy.

High bin resolution may be required for other microphysical processes besides condensation/evaporation. In particular, the aggregation process is important for large raindrops and ice crystals. Therefore, the method outlined here might be expected to allow the bin resolution to be reduced over the range of small particles, but not over the range of large particles.

ACPD
11, 21631–21654, 2011

References

Chen, J. P. and Lamb, D.: Simulation of cloud microphysical and chemical processes using a multicomponent framework. Part I: Description of the microphysical model, J. Atmos. Sci., 51, 2613–2613, doi:10.1175/1520-0469(1994)051<2613:SOCMAC>2.0.CO;2, 1994. 21632, 21634, 21636, 21645

Chen, J. P. and Lamb, D.: Simulation of cloud microphysical and chemical processes using a multicomponent framework. Part II: Microphysical evolution of a wintertime orographic cloud, J. Atmos. Sci., 56, 2293–2312, doi:10.1175/1520-0469(1999)056<2293:SOCMAC>2.0.CO;2, 1999. 21632

Dinh, T., Durran, D. R., and Ackerman, T.: Maintenance of tropical tropopause layer cirrus, J. Geophys. Res., 115, D02104, doi:10.1029/2009JD012735, 2010. 21632

Hashino, T. and Tripoli, G. J.: The spectral ice habit prediction system (SHIPS). Part I: Model description and simulation of the vapor deposition process, J. Atmos. Sci., 64, 2210–2237, doi:10.1175/JAS3963.1, 2007. 21632

Kuba, N. and Fujiyoshi, Y.: Development of a cloud microphysical model and parameterizations to describe the effect of CCN on warm cloud, Atmos. Chem. Phys., 6, 2793–2810, doi:10.5194/acp-6-2793-2006, 2006. 21632

Kuba, N. and Murakami, M.: Effect of hygroscopic seeding on warm rain clouds - numerical study using a hybrid cloud microphysical model, Atmos. Chem. Phys., 10, 3335–3351, doi:10.5194/acp-10-3335-2010, 2010. 21632

Lin, R.-F., Starr, D. O., Reichardt, J., and DeMott, P. J.: Nucleation in synoptically forced cirrostratus,, J. Geophys. Res, 110, D08208, doi:10.1029/2004JD005362, 2005. 21632

Pruppacher, H. R. and Klett, J. D.: Microphysics of Clouds and Precipitation, D. Reidel Publishing Company, Dordrecht, Holland, 1978. 21643

Przyborski, P.: Goddard Cumulus Ensemble model, ONLINE, http://atmospheres.gsfc.nasa.gov/cloud_modeling/models_gce.html, 2006. 21632

Tzivion, S., Feingold, G., and Levin, Z.: The evolution of raindrop spectra. Part II: Collisional collection/breakup and evaporation in a rainshaft., J. Atmos. Sci., 46, 3312–3328, doi:10.1175/1520-0469(1989)046<3312:TEORSP>2.0.CO;2, 1989. 21641

ACPD
11, 21631–21654, 2011

Table 1. Root-mean-square errors in the number of drops (10^6 m^{-3}) of the solutions at 50 min obtained by the linear and cubic schemes in the evaporation problem.

Number of bins	Linear	Cubic
10	2.9918	2.1007
20	1.2199	0.6424
40	0.1343	0.0556
60	0.0221	0.0093
80	0.0062	0.0039

ACPD
11, 21631–21654, 2011

Table 2. Root-mean-square errors in the number of crystals (10^3 m^{-3}) of the solutions at 30 min obtained by the linear and cubic schemes in the depositional growth problem.

Number of bins	Linear	Cubic
6	9.5707	2.8722
8	3.7011	1.5335
10	1.7659	0.5899
12	0.9428	0.2665
16	0.3377	0.0804
20	0.1486	0.0346

ACPD
11, 21631–21654, 2011

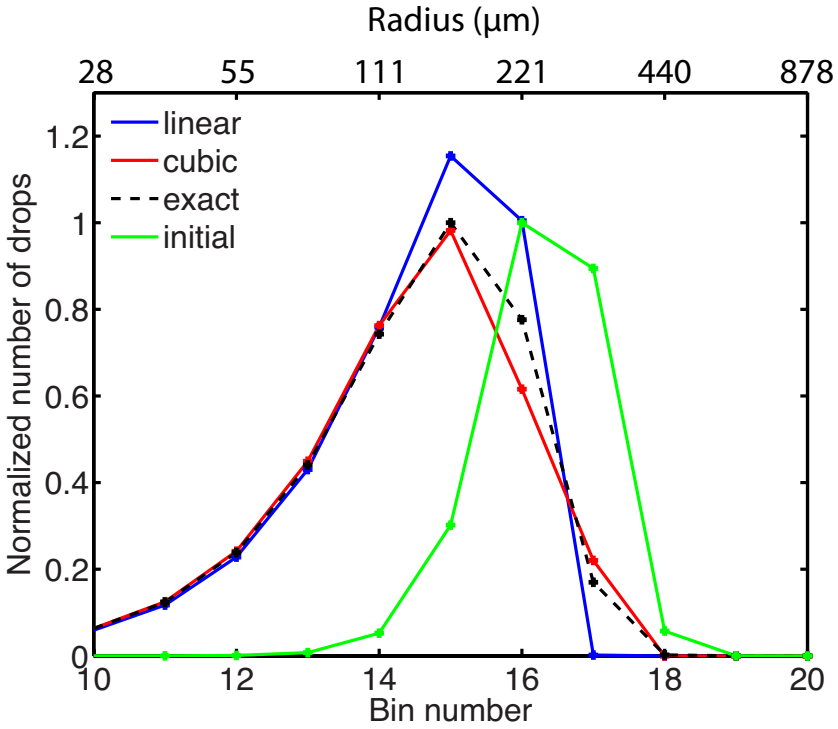

Fig. 1a. The analytical solution and numerical solutions obtained by the linear and cubic schemes at 20-bin-resolution at 50 min in the evaporation problem. The initial and final numbers of drops per bin are normalized by the exact maximum numbers at respectively the initial time (see Eq. 24) and the final time (see Eq. 25). The radii corresponding to the masses at the bin centers are indicated at the top of the plot.

ACPD
11, 21631–21654, 2011

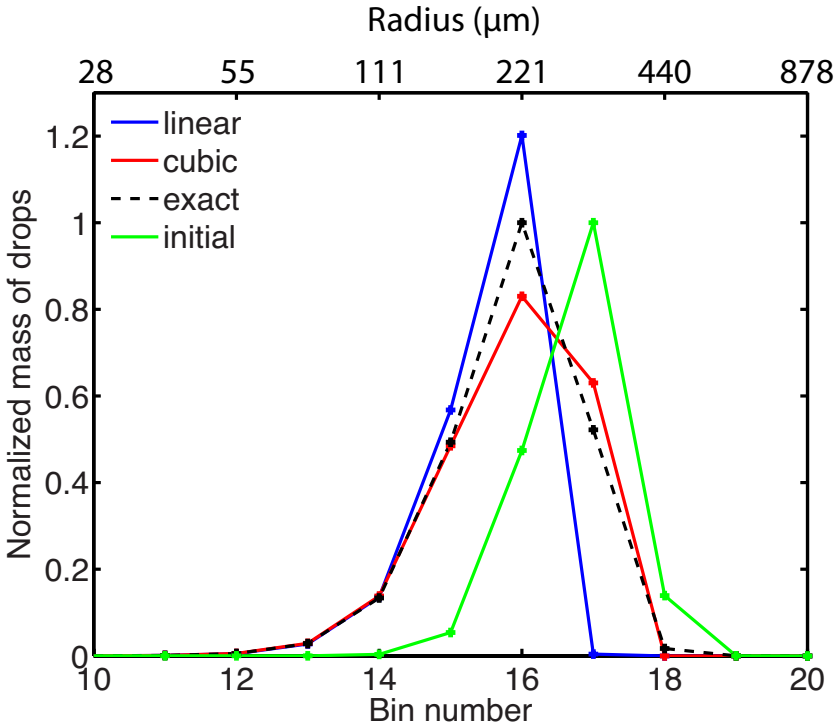

Fig. 1b. The analytical solution and numerical solutions obtained by the linear and cubic schemes at 20-bin-resolution at 50 min in the evaporation problem. The initial and final masses of drops per bin are normalized by the exact maximum masses at respectively the initial time (see Eq. 24) and the final time (see Eq. 25). The radii corresponding to the masses at the bin centers are indicated at the top of the plot.

ACPD
11, 21631–21654, 2011

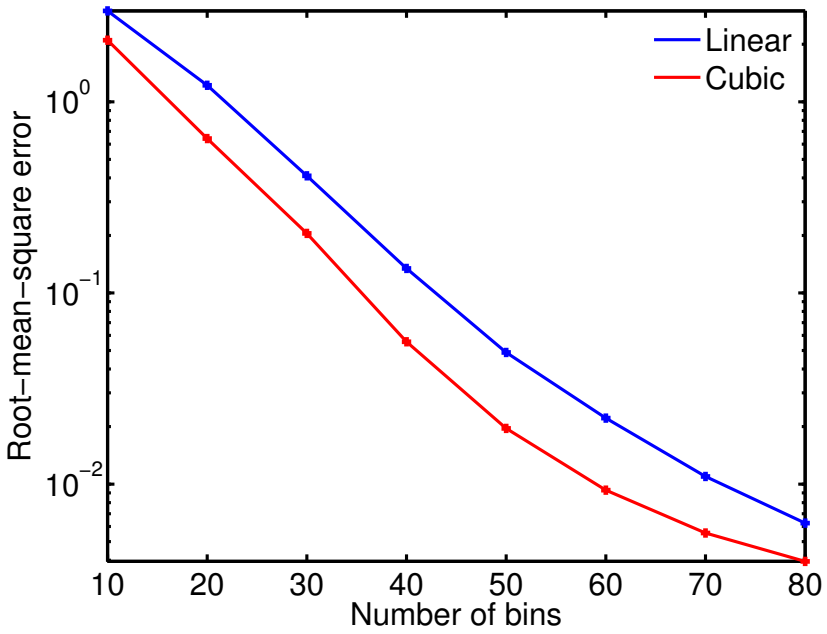

Fig. 2. Root-mean-square errors in the number of drops (10^6 m^{-3}) of the solutions at 50 min obtained by the linear and cubic schemes in the evaporation problem.

ACPD
11, 21631–21654, 2011

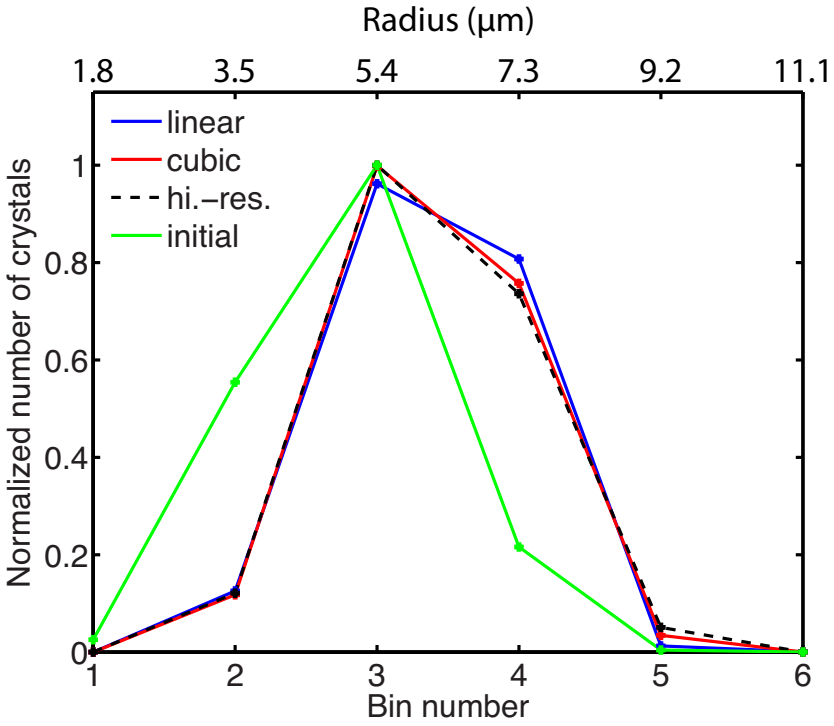

Fig. 3a. Numerical solutions obtained by the linear and cubic schemes at 30 min in the depositional growth problem. The low resolution solutions (blue and red curves) are obtained at 6-bin-resolution. The high resolution solution (black, dashed curve) is obtained at 200-bin-resolution. The initial and final numbers are normalized by the maximum numbers at respectively the initial and final time of the high resolution solution. The radii corresponding to the masses at the bin centers are indicated at the top of the plot.

ACPD
11, 21631–21654, 2011

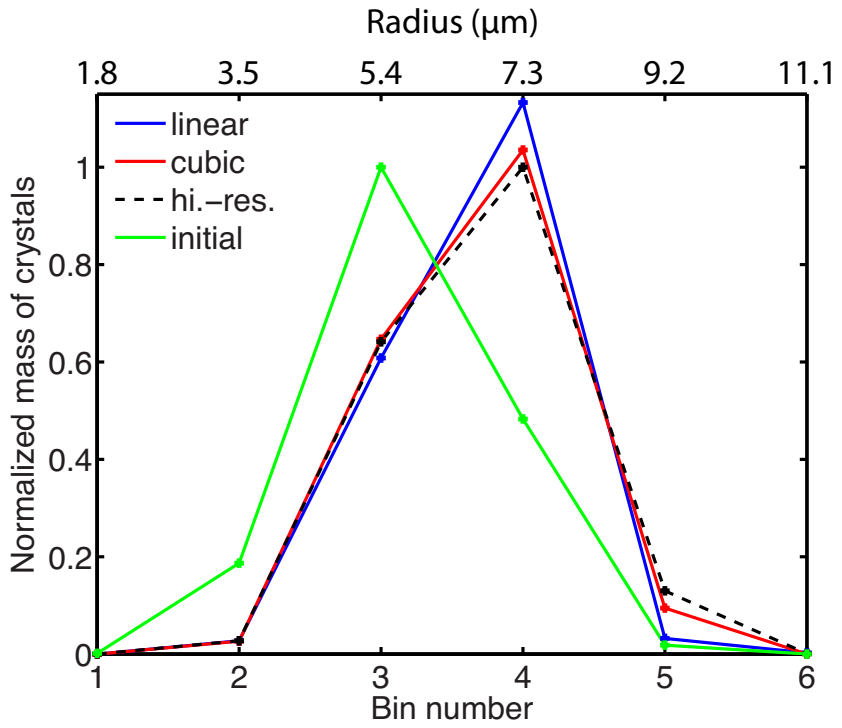

Fig. 3b. Numerical solutions obtained by the linear and cubic schemes at 30 min in the depositional growth problem. The low resolution solutions (blue and red curves) are obtained at 6-bin-resolution. The high resolution solution (black, dashed curve) is obtained at 200-bin-resolution. The initial and final masses are normalized by the maximum masses at respectively the initial and final time of the high resolution solution. The radii corresponding to the masses at the bin centers are indicated at the top of the plot.

ACPD
11, 21631–21654, 2011

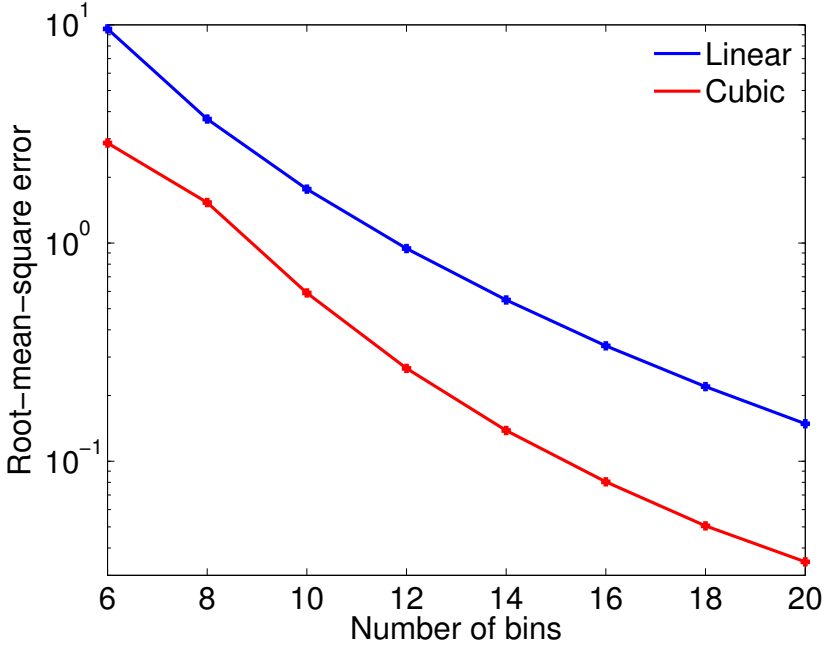

Fig. 4. Root-mean-square errors in the number of crystals (10^3 m^{-3}) of the solutions at 30 min obtained by the linear and cubic schemes in the depositional growth problem.

ACPD
11, 21631–21654, 2011